Distinct wind convergence patterns due to thermal and momentum forcing of the low level jet into the Mexico City basin

B. de Foy, A. Clappier, L. T. Molina, M. J. Molina

Atmos. Chem. Phys. Discuss., 5, 11055–11090, 2005
www.atmos-chem-phys.org/acpd/5/11055/
SRef-ID: 1680-7375/acpd/2005-5-11055
European Geosciences Union

Atmospheric Chemistry and Physics Discussions

Distinct wind convergence patterns due to thermal and momentum forcing of the low level jet into the Mexico City basin

B. de Foy[1], **A. Clappier**[2], **L. T. Molina**[1], **and M. J. Molina**[1]

[1]Department of Earth, Atmospheric and Planetary Sciences, Massachusetts Institute of Technology, USA
[2]Air and Soil Pollution Laboratory, Swiss Federal Institute of Technology, Lausanne (EPFL), Switzerland

Received: 7 October 2005 – Accepted: 17 October 2005 – Published: 1 November 2005

Correspondence to: B. de Foy (bdefoy@ucsd.edu)

Abstract

Mexico City lies in a high altitude basin where air quality and pollutant fate is strongly influenced by local winds. The combination of high terrain with weak synoptic forcing leads to weak and variable winds with complex circulation patterns. A low level jet entering the basin in the afternoon leads to very different wind convergence lines over the city depending on the meteorological conditions. Surface and upper-air meteorological observations are analysed during the MCMA-2003 field campaign to establish the meteorological conditions and obtain an index of the strength and timing of the jet. A mesoscale meteorological model (MM5) is used in combination with high-resolution satellite data for the land surface parameters and soil moisture maps derived from diurnal ground temperature range. A simple method to map the lines of wind convergence both in the basin and on the regional scale is used to show the different convergence patterns according to episode types. The low level jet is found to occur on most days of the campaign and is primarily due to thermal forcing which is very similar from day to day. Momentum mixing from winds aloft into the surface layer is much more variable and can determine both the strength of the jet and the pattern of the convergence zones. Northerly flows aloft lead to a weak jet with an east-west convergence line that progresses northwards in the late afternoon and early evening. Westerlies aloft lead to stronger jets and a north-south convergence line through the middle of the basin starting in the early afternoon. Improved understanding of basin meteorology will lead to better air quality forecasts for the city and better understanding of the chemical regimes in the urban atmosphere.

1. Introduction

The interaction of a low level jet with regional air flows into the Mexico City basin leads to complex convergence patterns that determine the concentration and fate of air pollutants, with strong associated health effects. Stensrud (1996) reviews the climatological

ACPD

5, 11055–11090, 2005

importance of low level jets, summarising research on several categories of jets including those due to terrain effects. Kimura and Kuwagata (1993) study in greater detail the thermal forcing in an elevated basin, leading to low pressures and a strong flow over from neighbouring valleys over mountain ridges. Optimum conditions are a basin less than 100 km and mountain ranges slightly lower than the mixing height, both of which are satisfied by the Mexico City basin. Banta and Cotton (1981) analysed the structure of the local wind systems in a broad mountain basin and found that in addition to night-time drainage and day-time up-slope flows, there were afternoon winds due to down-mixing of momentum aloft into the boundary layer.

A number of recent field campaigns have taken place in mountain valleys and basins. The Vertical Transport and Mixing (VTMX, Doran et al., 2002) field campaign studied the meteorological processes in Salt Lake city in October 2002. Banta et al. (2004) found that cold drainage flows from the surrounding mountains could lead to convergence in the basin and vertical motion within a cold stable atmosphere. Rife et al. (2004) looked at the performance of a range of mesoscale meteorological models for the complex local flows measured during VTMX. They found that by standard verification measures, high resolution models did not perform significantly better than the regional models. This was traced to the high fraction of spectral power in the subdiurnal range which the models cannot simulate exactly. Accounting for this however suggests that the high resolution models do perform better.

The Mesoscale Alpine Programme (MAP, Mayr et al., 2004) provided extensive measurements in a gap through the Alps. The aim of the study is to study the interaction of the gap flow with the flow aloft, develop local forecasting methods and improve model verification. Zängl et al. (2004) developed the MM5 model to use true horizontal diffusion. This lead to improved simulations of the progression of the Foehn down the valley and its impact on the cold air pool at Lake Constance due in part to the improved modelling of the vertical turbulent mixing. Liu et al. (2000) describe a different low level jet in Iran where a synoptic surface high leads to an outflow of cold air down valley. The strength of the jet is determined by the balance of the pressure, momentum and

ACPD
5, 11055–11090, 2005

friction forces.

Kossmann and Fiedler (2000) analysed the diurnal momentum budget of thermally induced slope winds. The balance between the buoyancy and pressure gradient forces with the friction forces was found to determine the strength of the slope flows. These were also found to react to changes of forcing within 120 s. The formation of a mesoscale heat low was described by Kossmann et al. (2002) in an alpine lake basin. This is similar to Kimura and Kuwagata (1993) and leads to an intrusion of cold air into the basin in the late afternoon. Regmi et al. (2003) find a similar situation in Kathmandu, Nepal. Shallow surface influx of cool south-westerly air from the Indian plateau forms a stable layer beneath north-westerly valley flow. The resulting layers suppress vertical mixing and lead to high air pollution events.

As reviewed in Molina and Molina (2002), the Mexico City Metropolitan Area (MCMA) lies in a dry lake bed surrounded by high mountains and suffers from high levels of air pollution. Bossert (1997) modelled the local wind circulation and showed distinct pollution venting patterns depending on the interaction of the synoptic and local winds. Jazcilevich et al. (2003) examine cases of convective transport of pollutants in the basin and the flushing of pollutants through the passage to the south-east. The IMADA-AVER field campaign (Doran et al., 1998) made extensive meteorological observations in the basin and found large day-to-day variation in the wind patterns. Fast and Zhong (1998) describe in detail some of the wind patterns leading to high surface ozone concentrations, including the presence of a convergence zone that moves through the MCMA from south to north. Whiteman et al. (2000) analyse the heat budget in the basin to highlight the importance of an influx of cool moist air through the Chalco gap in the south-east of the basin, similar to the flows described by Kimura and Kuwagata (1993). Doran and Zhong (2000) analyse this gap flow in terms of the heat balance on the regional scale and across the basin rim to find that the jet strength is a function of the thermal forcing.

de Foy et al. (2005a) analyse the meteorological conditions during the MCMA-2003 field campaign. Three different wind circulation episode types are proposed for the

duration of the campaign. O3-South are days when ozone is high in the south and a weak late afternoon jet flow forms. O3-North days are when the ozone peak is in the north due to the combination of a strong jet and flow over the south and west edges of the basin. Cold Surge days are when cold northerlies sweep the basin atmosphere clean.

This paper adopts the analysis of Doran and Zhong (2000) for the wind jets occurring during MCMA-2003, classifying the results according to the three episode types. Convergence zones suggested by Fast and Zhong (1998) are shown explicitly thereby illustrating the interaction of synoptic and local scales proposed by Bossert (1997).

After describing the observations and model used in Sect. 2, the synoptic conditions during MCMA-2003 will be reviewed in Sect. 3 and the model results will be evaluated in Sect. 4. Sections 5 and 6 will describe the low level jet and the convergence patterns. Section 7 will discuss how the circulation patterns relate to the local and synoptic forcings.

2. Observations and model description

The observations described in de Foy et al. (2005a) are used, in particular the surface meteorological observation network and the radiosondes of the Mexican National Weather Service (Servicio Meteorológico Nacional, SMN) and the monitoring data from the campaign super-site at the National Centre for Environmental Research and Training (Centro Nacional de Investigación y Capacitación Ambiental, CENICA) as well as the surface ozone measurements from the Ambient Air Monitoring Network (Red Automática de Monitoreo Atmosférico, RAMA). Figure 1 shows the radiosonde and surface stations along with geographical reference points. Figure 2 shows the basin topography and the urban area along with the stations in the MCMA. All times in this paper are stated as local time, per field campaign guidelines, which is Central Daylight savings Time (CDT=UTC–5 h).

The basin circulation is simulated using the Pennsylvania State University/National

ACPD
5, 11055–11090, 2005

Center for Atmospheric Research Mesoscale Model (MM5, Grell et al., 1995) version 3.7.2 using three nested grids with one-way nesting. The grid resolution used is 36, 12 and 3 km, with 40×50, 55×64 and 61×61 grid cells for domains 1, 2 and 3, respectively. The simulation procedure is described in detail in de Foy et al. (2005b) and makes use of high resolution satellite remote sensing for initialising the land surface parameters. Nine simulations of 4 days were used to cover the entire field campaign, with the following two modifications. The initialisation period was increased from 18 to 42 h, yielding better results for the first simulation day.

Due to an unverified moistening of the soil in the AGRMET model half-way during the campaign, the previous modelling study made use of averaged AGRMET soil moisture during the first part of the month which were held constant during the simulation. This method fails to capture the variation of the soil moisture during the field campaign. Soil moisture products are available from AMSR-E. These are valid for a very thin surface layer. In this case, the top layer is very dry and does not reflect the moisture below the soil. An alternative was therefore obtained by relating the soil moisture to the diurnal range of the skin temperature measured by MODIS on the AQUA platform. 8-day average values were used for the months of March–May 2003. An empirical relationship was devised to produce fields of similar magnitudes to those from AGRMET. Soil temperature differences in the range of 15 K to 45 K were linearly mapped to soil moistures of 0.18 to 0.08 m^3/m^3 for the surface layer, 0.22 to 0.12 for layer 2 and 3 and 0.3 to 0.2 for layer 4 (i.e. points with the largest diurnal temperature range have the driest soils). Gaussian smoothing was applied to all the fields; one pass for layers 1 and 2, two passes for layers 3 and 4. Initial fields were interpolated in time from the 8-day estimated values, and were held constant in the MM5 simulation. This scheme improves the simulation of the diurnal temperature range and also captures some soil moisture variation during the campaign. The eight day smoothing on the soil temperature however leads to an under estimation of the soil moisture variability. This could be an important factor in the simulation of the Cold Surge episodes which would merit further analysis.

ACPD
5, 11055–11090, 2005

3. Synoptic conditions

Synoptic weather charts for the 3 episode types were shown in de Foy et al. (2005a). Cold Surge episodes are due to a surface high over Texas with a low pressure system aloft. O3-South episodes occur when a anti-cyclone is over Mexico and O3-North when low pressure systems move north of the MCMA forcing the sub-tropical jet southward. In order to compare all the days of the campaign with the synoptic charts, Fig. 3 shows the evolution of the 500 hPa height and temperature at radiosonde locations on the coasts and in Mexico City.

The most variability occurs at Brownsville where the high pressure for O3-South days can be clearly seen. O3-North episodes are characterised by a north-south pressure gradient which drives the westerlies aloft and Cold Surge episodes by falling pressure at most of the stations. The temperature at 500 hPa is high and rising for O3-South days, constant with a stronger north-south gradient for O3-North days and decreasing for Cold Surge days.

Daily average surface pressure and temperature are shown in Fig. 4. High surface pressures at Matamoros and Veracruz during Cold Surge episodes force cold northerly surface flows. O3-South days have minimal pressure gradients between the two coasts with increasing surface temperatures. On O3-North days the pressure on the Gulf coast tends to be lower than on the Pacific Coast.

From this, it is clear that the three Cold Surge episodes follow the pattern described by Schultz et al. (1998), with varying intensities. Both the O3-South and O3-North episodes, with the exception of the transition periods, have well defined synoptic characteristics that vary little across the different days.

4. Model results

Model statistics were calculated for each simulation for the SMN weather stations in the basin. Figure 5 shows the centred root mean square error (RMSEc) versus the bias

ACPD
5, 11055–11090, 2005

along side the model versus observed standard deviation of the data for temperature, humidity and wind speed, as described in de Foy et al. (2005b). Temperature biases are less than 1 K with the exception of the first Cold Surge episode. RMSEc are within 2 K with the exception of the first two Cold Surge episodes. For water mixing ratio, the biases are within 1.5 g/kg and the RMSEc in the range of 1 to 2 g/kg, although the first Cold Surge episode is too moist and has larger errors than the other simulations. Wind speed performance is similar for all the simulations with the exception of the second Cold Surge episode when the winds are too strong and the errors largest. Overall, this suggests that the simulation performance for the whole campaign is similar to that of the O3-South episode described in de Foy et al. (2005b). The Cold Surge episodes are an exception to this however and would need further refinement, probably in the soil moisture field.

Continuous time series for the field campaign were obtained by collating the results from the nine simulations. Figure 6 shows the diurnal variation of the model winds at CENICA by episode. For each episode, the median is shown by a bold line, the inter-quartile range by thin lines and the total range by dotted lines. The winds are south-easterly and below 2 m/s in the early morning turning to northerly during the day and then back to southerly in the range of 4 to 6 m/s by sunrise. Comparison with Fig. 8 in de Foy et al. (2005a) shows that the main features are well represented by the model. O3-North episodes have a stronger and earlier wind speed peak whereas Cold Surge winds are slightly weaker. The main difference between the model and the observations is the delay in the increase in wind speeds. Whereas the observed winds increase linearly starting at 09:00, the model increase starts after 12:00 and is much steeper. In terms of wind directions, the main feature of the observations is the afternoon wind shift which takes place around 15:00 for O3-North, around 20:00 for O3-South and around 04:00 for Cold Surge. The model simulates this although the difference between O3-North and O3-South is not as stark. In the morning there is a sharp transition from south-easterly to north-westerly whereas the observations show a more gradual turning via the east. In the afternoon there is a large variability in the

ACPD
5, 11055–11090, 2005

Cold Surge winds with a southerly component which the observations do not show. The Cold Surge episode type contains the greatest variation of circulation patterns and in addition is the least well simulated of the three types. Nevertheless, the afternoon wind direction is better simulated at stations further from the Chalco gap in the south-east – both in the city and to the east of the basin at Chapingo – suggesting that this is due to the gap flow intensity.

5. Low level jet

The wind shifts observed at CENICA are part of the low level jet that passes through the Chalco passage, as described in Whiteman et al. (2000). Figure 7 shows the surface winds in the basin for selected days of the three episode types at 16:00 and 19:00.

O3-South days such as 16 April have weaker northerly winds and a gap flow influencing the south-east of the city in the early evening. 23 April, an O3-North day, has a gap flow that is already influencing the whole eastern half of the basin by 16:00. It meets with westerly winds coming over the basin rim leading to a convergence line in the middle of the city. This is pushed further north as the afternoon progresses. On this particular day, the convergence leads to strong convection and cloud formation causing highly variable surface winds. On 9 April, a Cold Surge day, strong northerly flows are forced into the gap and are followed by a shift to westerly winds throughout the basin.

North-south cross-sections through the Chalco gap in Fig. 8 show the horizontal winds and contours of potential temperature. On O3-South days the winds aloft are weaker. Westerlies above 6000 m give way to northerly winds below. A strong temperature gradient forms between the basin and the Cuautla valley to the south. The associated pressure difference drives a low level jet less than 1000 m thick which brings in cold air. The jet progresses gradually through the basin turning to easterly as it meets the northerly flow in the basin. On O3-North days, the winds aloft are still from the west, but stronger and with no layer of northerlies below. The potential temperature difference between the basin and the valley to the south, at 6 K, is the same as 16 April.

ACPD
5, 11055–11090, 2005

The low level jet however is much stronger and deeper. By 16:00 it is nearly 2000 m thick and extends all the way to the northern edge of the basin. By 19:00, horizontal convergence of winds leads to strong convective activity and the formation of cumulus clouds in the north of the basin. Cold Surge days have strong westerly winds aloft with north-easterlies entering the basin from the Gulf coast. At 16:00 the model simulates a limited low level jet which meets the moist Gulf air leading to westerly winds into the early evening.

6. Wind convergence

6.1. Convergence patterns from model simulations

The formation of low level jet winds and of terrain induced circulations leads to convergence zones in the basin. On the regional scale, convergence zones are also formed due to the opposite flows from the sea breezes of the Pacific Ocean and of the Gulf of Mexico. These can be diagnosed by looking at vertical velocities above a given threshold, chosen to be 0.5 m/s. For each column, the values at sigma level 17 were chosen as this corresponds to roughly 1300 m above ground level which is either above or towards the top of the surface layer.

Figure 11 shows such a plot for the medium and fine domains, with convergence zones for a whole day coloured by time of day. O3-South days have weak synoptic forcing and a much clearer signature of terrain induced flow. On the regional scale, convergence lines are formed from the meeting of the sea breezes from the Pacific and the Gulf. These are relatively stationary moving south-west only slightly during the afternoon. The combination of terrain blocking from the east-west range of volcanoes forming the south of the basin and the flat mexican plateau to the north of the basin leads to an advance of the convergence line which now passes through the MCMA. On the basin scale, the low level jet coming from the Chalco passage forms a very clear signature, starting at 15:00 and sweeping through the whole city by 22:00. Similar jets

ACPD
5, 11055–11090, 2005

can be seen through Toluca to the west and past Puebla on the east, due to the same terrain elevation differential between the plateaus to the north and the low-lying Cuautla valley to the south.

On O3-North days, the regional convergence line is now at the edge of the Sierra Madre Oriental, due to the strength of the westerlies. In the basin, the low level jet is much stronger and leads to an early convergence zone that runs north-south through the centre of the city. On 23 April, the meeting point of the gap flow and the winds coming over the basin rim exhibits some meandering in the north-west of the basin. In addition, later afternoon convection can be seen as east-west lines across the basin. For 24 April however there were no clouds and the convergence line is quite stationary. Three air masses can be seen pushing into the basin: the gap flow from Chalco, the westerlies over the Toluca pass to the west and the flow over the Ajusco mountain to the south.

For 8 April, strong cold northerly winds from the Gulf lead to up-slope flows on the edge of the Sierra Madre Oriental. The winds then continue over the Mexican plateau and highlands meeting in a convergence zone nearer to the Pacific coast. In the basin, the situation is complicated with strong convective activity in the basin and slope flows on the basin edge. On 9 April, drier conditions lead to reduced convection and a clearer convergence zone along the south-west of the country. In the basin, we now see the convergence lines due to the low level jet radiating from the Chalco passage. These are limited in both time and space however, with late afternoon convergence above the mountains.

6.2. Verification with surface ozone and cloud imagery

Verification of the convergence lines is difficult to achieve by comparisons with instantaneous observed winds. Their impact on the basin circulation can be seen however by looking at the transport of pollutants and water vapour. The maximum daily ozone measured by RAMA in the MCMA along with a GOES visible image taken in the afternoon are shown alongside the convergence patterns in Fig. 11.

ACPD
5, 11055–11090, 2005

O3-South days have high ozone peaks in the south-west, as would be predicted from the convergence patterns. In particular, ozone is higher on 16 April than on 15 April due to the delayed gap flow. The Goes image shows very clearly the low level clouds on the Gulf coast plains due to the sea breeze. Scattered cloud formation is limited to the high volcanoes due to the dry prevailing conditions.

On O3-North days the ozone peak is in the north-west of the city, due to the gap flow pushing all the pollutants back through the basin to the north-west. The peaks are equivalent for 23 and 24 April, but on the 23 the spatial extent is larger and on the 24 the peak is further to the east. This is in accordance with the convergence lines that are meandering over the north-west on the first day, and oriented towards the north-east with stronger westerlies flushing the basin on the second day. There is much less cloudiness on the plains from gulf breezes, but there is convection on the edge of the Sierra Madre Oriental, as suggested by the convergence lines that are very sharply located over the ridge. Afternoon convection in the basin can be clearly see on 23 April, whereas 24 April has clear skies.

Cold Surge days have low ozone levels with maxima in the south of the basin, confirming wind transport to the south. On 8 April, ozone peaks are in the south-west in accordance with early afternoon convergence resulting from northerly flow meeting the Ajusco mountain. On 9 April, the peak is to the south-east which is where a small gap flow is forming owing to the clearer sky conditions on this day. Cloud transport to the eastern flanks of the Sierra Madre Oriental shows the northerly flows, followed by strong convection over the Mexican plateau and above the basin once the winds pass over the mountain edge.

7. Discussion

The Froude number determines the impact of complex terrain on wind circulation. The Brunt-Väisälä frequency was calculated from model output and found to be in the range of 0.005 to 0.015 s^{-1} over the basin. Taking a mean free velocity of 10 m/s as repre-

ACPD
5, 11055–11090, 2005

sentative of the conditions near the mountain tops, and distances of 1000 and 1500 m as representative of the mountain ridge heights above basin level on the eastern and western side yielded Froude numbers in the range of 2.8 to 12.5, see Table 1. Because these are always greater than one, the wind flow can be expected to be over the mountain tops with limited mountain waves. The primary effect of the mountains is therefore due more to the generation of up-slope and drainage flows rather than to the disruption of the mean tropospheric flow.

During the IMADA campaign, the jet strength through the Chalco passage was diagnosed from wind profiler data (Doran and Zhong, 2000). As no such data is available during the MCMA-2003, an alternative was sought that would be based on routine surface observations in the basin. A simple metric was devised based on southerly component of velocity in the basin above a threshold of 1 m/s. The excess velocity above the threshold was summed between 12:00 and 24:00 and divided by an average estimated jet length of 6 hours. The average was then taken over the 5 SMN stations to yield a number that can be roughly interpreted as an excess meridional wind speed due to the jet flow. The average time of the jet was obtained by averaging the time of day weighted by the jet strength for every hour at each station. Figure 12 shows the jet strength versus the jet time for the observations and for the model simulations for each day of the campaign. The three episode types are clearly segregated into three separate categories. Weak and early jets for Cold Surge days, weak and later jets for O3-South days and strong jets peaking around 18:00 for O3-North. The model reproduced this pattern although the O3-North days tend to be weaker and the O3-South and Cold Surge days too strong. Individual timing of the jet can be off by up to 3 hours or more, but overall, the simulations are within 1 to 2 hours of the observations.

The Mexico City basin has surface wind speeds below 1 m/s during the early morning leading to very stagnant air masses. Because the basin is at low latitude and high altitude, solar heating is intense and develops rapidly after sunrise, leading to a rapid growth of the boundary layer. The valley to the south of the basin, at an elevation of 1000 m a.s.l., is 1200 m below the basin level. The first effect of this is that in the bot-

ACPD
5, 11055–11090, 2005

tom 2000 m layer of the atmosphere there are roughly 1400 kg/m^2 of air at CENICA but 1720 kg/m^2 at Cuautla. For equivalent surface heating, this leads to an average diurnal temperature variation at CENICA of 5 K and at Cuautla of 3.5 K. Because this leads to lower mixing heights at Cuautla, the temperature at equivalent heights is higher at CENICA, leading to temperature gradients between CENICA and Cuautla in the 2250 to 3250 m a.s.l. range of around 5 K.

Doran and Zhong (2000) analysed jet strength as a function of two different temperature differentials. The first was the average temperature difference in the range of 2800 to 3200 m a.s.l. between the Tres Marias site on the southern basin rim and the average of 3 radiosondes in the basin at 13:30 CST. The second was the average difference in temperature in the range of 2250 to 3150 m a.s.l. between the Mexico City and Acapulco radiosondes at 18:00 CST. A correlation was found between strong jets and large temperature gradients suggesting thermal forcing as the main cause of the jets.

During MCMA-2003, there were no Acapulco soundings at 19:00. Analysing previous soundings shows however that there is little difference in temperature at that height range between the 07:00 and 19:00 soundings. Furthermore, there is little difference between the Acapulco and Mexico City soundings for this same height range at 07:00. The temperature difference is therefore a proxy for the heating at the Mexico City radiosonde site during the day. Figure 13 plots the jet strength versus the temperature difference in the bottom 1000 m layer above ground level at GSMN between the 07:00 and 19:00 soundings. Substantial heating takes place on nearly all of the days. There is a clear difference between the Cold Surge days with small temperature differences and the O3-South days with larger differences. Overall however there is no clear correlation between jet strength and temperature difference.

The temperature difference between Tres Marias and the basin during IMADA served as a more direct measure of possible thermal forcings. As this was unavailable, the simulated temperature difference was calculated between CENICA, which is near the geographic centre of the basin, and Cuautla just to the south of the Chalco passage for

the same vertical interval (2250 to 3250 m a.s.l.) at 15:00, as shown in Fig. 13. Table 2 shows the parameters for a linear fit to the data by episode. For O3-South episodes there is a positive correlation of temperature gradient and jet strength that explains 16% of the variance. For O3-North days however, there is zero correlation.

Episode types in the basin were found to correlate with wind direction aloft. The jet strength was therefore plotted versus average wind direction at the top of the boundary layer (4250 to 6250 m a.s.l.) for the 07:00 sounding, shown in Fig. 14. For the 4 cases where the 07:00 sounding was missing, data was taken from the 13:00 or 19:00 sounding depending on availability. For O3-South days, this shows a clear negative correlation with northerly winds aloft causing weaker jets and westerlies causing stronger jets. The linear fit explains 84% of the variation. For O3-North days there is little variation in the wind direction and a slight negative correlation that explains only 5% of the variation. The correlation between the jet strength and the wind direction aloft is in accordance with Banta and Cotton (1981). They describe the influence of wind direction aloft on basin winds in South Park, Colorado as the mixing layer causes momentum exchange with the surface layer leading to "afternoon westerlies" in the basin. This suggests that the winds aloft and the location of the regional convergence zone will have a predictable impact on the balance between the different flows into the Mexico City basin.

On O3-South days, the regional convergence line passes through the basin starting on the east side and moving to the west side in the afternoon. This leads to air masses from the Mexican plateau entering the basin in the morning giving way to Gulf air as the convergence line moves west. The weak westerlies aloft give way to an intermediate layer of northerly flow. As the basin air heats up relative to surrounding air masses, the low level jet from the Cuautla valley enters the basin pushing back the northerlies, with the location of the convergence line between the two determined by the balance between the momentum down-mixing and the thermally-induced pressure low.

On O3-North days, the regional convergence is to the east of the basin on the edge of the Sierra Madre Oriental. This leads to stronger westerlies aloft and surface norther-

ACPD
5, 11055–11090, 2005

lies from the Mexican plateau in the morning. In the afternoon, the low level jet coming from the south-east meets with air masses that are pushed over the southern and western edges of the basin rim by the westerlies aloft. Together, these 3 fluxes into the basin flush out the basin to the north-west.

Cold Surge days are characterised by high surface pressures to the north and strong westerlies aloft. This leads to strong, cold, surface northerlies which are held back early in the day behind the Sierra Madre Oriental and then move through the Mexican plateau leading to regional convergence lines south-west of the basin. In the basin, the northerlies sweep through the MCMA and move south into the Chalco gap. Despite the cold temperatures and increased cloudiness, a weak afternoon low level jet still develops on most days. It does not progress through the basin however, turning west instead at east-west convergence lines. Convection develops along these lines with associated afternoon rainfall.

8. Conclusions

Wind circulation in the Mexico City basin is characterised by a low level jet coming through the mountain pass in the south-east and extending into the basin. This takes place nearly every day, with varying strength and depth. The main mechanism behind this is the thermal imbalance between the hot air in the basin and the cooler air in the low-lying valley to the south. This does not vary much from day to day however, and was shown to be a poor predictor of the jet strength. Wind direction aloft was shown to explain most of the jet strength for O3-South days. Both temperature gradients and wind directions are very similar for all O3-North days and are therefore not able to account for the jet strength. Identifying determining factors will require further analysis of the synoptic conditions and vertical mixing in the basin.

MM5 simulations were carried out for the whole campaign using high resolution satellite remote sensing of the land surface. Soil moisture fields were derived from the diurnal range of the ground temperature, leading to a spatially and temporally varying field.

ACPD
5, 11055–11090, 2005

Statistically, the model simulations were found to have low biases in surface temperature, humidity and wind speeds and errors in accordance with the episode discussed in de Foy et al. (2005b).

Wind convergence patterns over Mexico can be clearly identified by plotting the vertical velocity above a given threshold near the top of the surface layer. Combining these for every hour of the afternoon into a single map shows the development of the convergence zones. The Mexico City basin circulation was shown to depend on the interaction of two convergence zones: those resulting from the sea breezes from the Pacific Ocean and the Gulf of Mexico, and those formed from the interaction of a low level jet with northerly day-time winds in the basin. The resulting basin convergence patterns fit into the three episode types proposed in de Foy et al. (2005a). O3-South days have a convergence lines radiating northwards from the Chalco gap, moving through the basin in the late afternoon and early evening. O3-North days have north-south convergence lines through the middle of the MCMA due to the meeting of the gap flow with surface westerlies over the southern and western edges of the basin. Cold Surge days have east-west convergence line across the basin leading to cumulus convection and rainfall.

Verification of the convergence patterns was made possible by analysing surface ozone patterns in the basin and cloud formation observed by satellite. The spatial distribution of surface ozone can be clearly linked to the location of the afternoon convergence lines. Cloud patterns act as clear indicators of sea-breeze fronts and moist air movements over the mountains as well as convection lines in the basin. These were shown to correspond to the model simulated convergence lines on both the regional and local scale. An improved understanding of the transport processes in the Mexico City basin will improve air quality forecasts in the MCMA and the facilitate the evaluation of the regional impact of the MCMA plume. The increased understanding of the chemical regimes of the urban atmosphere will improve the evaluation of pollution control policies and the mitigation of health effects suffered by the people of the MCMA.

Acknowledgements. The analysis contained in this paper was made possible by the collabo-

rative efforts of many people involved in field measurements, both during the campaign and over longer periods of time. We are indebted to the staff of CENICA who hosted the campaign and would like to thank B. Cárdenas, S. Blanco, A. Sanchez, O. Fentanes, J. Zaragoza, A. P. Ocampo, C. Cruz, C. Aguirre, R. Romo, A. Pino, R. Castañeda, R. Rodríguez, P. Escamilla as well as R. Ramos, A. Retama and the operators and analyst personnel of the "Red Automática de Monitoreo Atmosférico del Gobierno del Distrito Federal" for their contribution in administering and gathering the data used in this manuscript. We are grateful to M. Rosengaus, J. L. Razo, J. Olalde and P. García of the Mexican National Meteorological Service for providing the EHCA and Radiosonde data.

MM5 is made publicly available and supported by the Mesoscale and Microscale Meteorology division at the National Center for Atmospheric Research. Their dedication and hard work is gratefully acknowledged. The satellite data used in this study were acquired as part of the NASA's Earth Science Enterprise. The algorithms were developed by the MODIS Science Teams. The data were processed by the MODIS Adaptive Processing System (MODAPS) and Goddard Distributed Active Archive Center (DAAC), and are archived and distributed by the Goddard DAAC.

We thank A. García and A. Jazcilevich of the Universidad Nacional Autónoma de México, A. Soler and F. Hernandez of the Secretaría del Medio Ambiente, Gobierno del Distrito Federal, México and J. Fast of Pacific Northwest National Laboratory for helpful discussions. The financial support from the US National Science Foundation (Award ATM-0511803), the US Department of Energy (Award DE-FG02-05ER63980), the Alliance for Global Sustainability and the Molina Center for Strategic Studies in Energy and the Environment for this work is gratefully acknowledged.

References

Banta, R. and Cotton, W. R.: An analysis of the structure of local wind systems in a broad mountain basin, J. Appl. Meteorol., 20, 1255–1266, 1981. 11057, 11069

Banta, R. M., Darby, L. S., Fast, J. D., Pinto, J. O., Whiteman, C. D., Shaw, W. J., and Orr, B. W.: Nocturnal low-level jet in a mountain basin complex. part I: Evolution and effects on local flows, J. Appl. Meteorol., 43, 1348–1365, 2004. 11057

Bossert, J. E.: An investigation of flow regimes affecting the Mexico City region, J. Appl. Meteorol., 36, 119–140, 1997. 11058, 11059

de Foy, B., Caetano, E., Magaña, V., Zitácuaro, A., Cárdenas, B., Retama, A., Ramos, R., Molina, L. T., and Molina, M. J.: Mexico City basin wind circulation during the MCMA-2003 field campaign, Atmos. Chem. Phys., 5, 2267–2288, 2005a, SRef-ID: 1680-7324/acp/2005-5-2267. 11058, 11059, 11061, 11062, 11071

de Foy, B., Molina, L. T., and Molina, M. J.: Satellite-derived land surface parameters for mesoscale modelling of the Mexico City basin, Atmos. Chem. Phys. Discuss., 5, 9861–9906, 2005b, SRef-ID: 1680-7375/acpd/2005-5-9861. 11060, 11062, 11071

Doran, J. C. and Zhong, S.: Thermally driven gap winds into the Mexico City basin, J. Appl. Meteorol., 39, 1330–1340, 2000. 11058, 11059, 11067, 11068

Doran, J. C., Abbott, S., Archuleta, J., Bian, X., Chow, J., Coulter, R. L., de Wekker, S. F. J., Edgerton, S., Elliott, S., Fernandez, A., Fast, J. D., Hubbe, J. M., King, C., Langley, D., Leach, J., Lee, J. T., Martin, T. J., Martinez, D., Martinez, J. L., Mercado, G., Mora, V., Mulhearn, M., Pena, J. L., Petty, R., Porch, W., Russell, C., Salas, R., Shannon, J. D., Shaw, W. J., Sosa, G., Tellier, L., Templeman, B., Watson, J. G., White, R., Whiteman, C. D., and Wolfe, D.: The IMADA-AVER boundary layer experiment in the Mexico City area, Bull. Amer. Met. Soc., 79, 2497–2508, 1998. 11058

Doran, J. C., Fast, J. D., and Horel, J.: The VTMX 2000 campaign, Bull. Amer. Met. Soc., 83, 537–551, 2002. 11057

Fast, J. D. and Zhong, S. Y.: Meteorological factors associated with inhomogeneous ozone concentrations within the Mexico City basin, J. Geophys. Res.-Atmos., 103, 18 927–18 946, 1998. 11058, 11059

Grell, G. A., Dudhia, J., and Stauffer, D. R.: A Description of the Fifth-Generation Penn State/NCAR Mesoscale Model (MM5), Tech. Rep. NCAR/TN-398+STR, NCAR, 1995. 11060

Jazcilevich, A. D., García, A. R., and Ruiz-Suarez, L. G.: A study of air flow patterns affecting pollutant concentrations in the Central Region of Mexico, Atmos. Environ., 37, 183–193, 2003. 11058

Kimura, F. and Kuwagata, T.: Thermally-induced wind passing from plain to basin over a mountain-range, J. Appl. Meteorol., 32, 1538–1547, 1993. 11057, 11058

Kossmann, M. and Fiedler, F.: Diurnal momentum budget analysis of thermally induced slope

ACPD

5, 11055–11090, 2005

winds, Meteorology Atmospheric Phys., 75, 195–215, 2000. 11058
Kossmann, M., Sturman, A. P., Zawar-Reza, P., McGowan, H. A., Oliphant, A. J., Owens, I. F., and Spronken-Smith, R. A.: Analysis of the wind field and heat budget in an alpine lake basin during summertime fair weather conditions, Meteorology Atmospheric Phys., 81, 27–52, 2002. 11058
Liu, M., Westphal, D. L., Holt, T. R., and Xu, Q.: Numerical simulation of a low-level jet over complex terrain in southern Iran, Mon. Weather Rev., 128, 1309–1327, 2000. 11057
Mayr, G. J., Armi, L., Arnold, S., Banta, R. M., Darby, L. S., Durran, D. D., Flamant, C., Gabersek, S., Gohm, A., Mayr, R., Mobbs, S., Nance, L. B., Vergeiner, I., Vergeiner, J., and Whiteman, C. D.: Gap flow measurements during the Mesoscale Alpine Programme, Meteorology Atmospheric Phys., 86, 99–119, 2004. 11057
Molina, L. T. and Molina, M. J. (Eds.): Air Quality in the Mexico Megacity, Kluwer Academic Publishers, 2002. 11058
Regmi, R. P., Kitada, T., and Kurata, G.: Numerical simulation of late wintertime local flows in Kathmandu valley, Nepal: Implication for air pollution transport, J. Appl. Meteorol., 42, 389–403, 2003. 11058
Rife, D. L., Davis, C. A., Liu, Y. B., and Warner, T. T.: Predictability of low-level winds by mesoscale meteorological models, Mon. Weather Rev., 132, 2553–2569, 2004. 11057
Schultz, D. M., Bracken, W. E., and Bosart, L. F.: Planetary- and synoptic-scale signatures associated with central American cold surges, Mon. Weather Rev., 126, 5–27, 1998. 11061
Stensrud, D. J.: Importance of low-level jets to climate: a review, J. Climate, 9, 1698–1711, 1996. 11056
Whiteman, C. D., Zhong, S., Bian, X., Fast, J. D., and Doran, J. C.: Boundary layer evolution and regional-scale diurnal circulations over the Mexico Basin and Mexican Plateau, J. Geophys. Res.-Atmos., 105, 10 081–10 102, 2000. 11058, 11063
Zängl, G., Chimani, B., and Häberli, C.: Numerical Simulations of the Foehn in the Rhine Valley on 24 October 1999 (MAP IOP 10), Mon. Weather Rev., 132, 368–389, 2004. 11057

Table 1. Froude numbers based on model Brunt-Väisälä frequency and representative mean velocity for mountain heights of 1000 m, representing the western ridge and 1500 m representing the volcanoes to the east.

$\overline{U}$	N_{bv}	$\lambda = \frac{2\pi\overline{U}}{N_{bv}}$	Froude No. $= \frac{\lambda}{h}$	
m/s	s^{-1}	m	h = 1000 m	h = 1500 m
	0.005	12 500	12.5	8.4
10	0.01	6300	6.3	4.2
	0.015	4200	4.2	2.8

ACPD

5, 11055–11090, 2005

Table 2. Least squares fit ($y=mx+c$) for correlation of jet strength with temperature gradient across the basin rim and wind direction aloft by episode type, with 95% confidence bound on m and correlation coefficient of the fit.

	ΔT vs. Jet Strength		WD vs. Jet Strength	
	O3-South	O3-North	O3-South	O3-North
m	0.23	−.01	−55	−7
95% bounds on m	−0.4, 0.8	−0.5, 0.5	−82, −28	−25, 11
c	5.1	5.3	24	−88
r^2	0.16	0.00	0.84	0.05

ACPD

5, 11055–11090, 2005

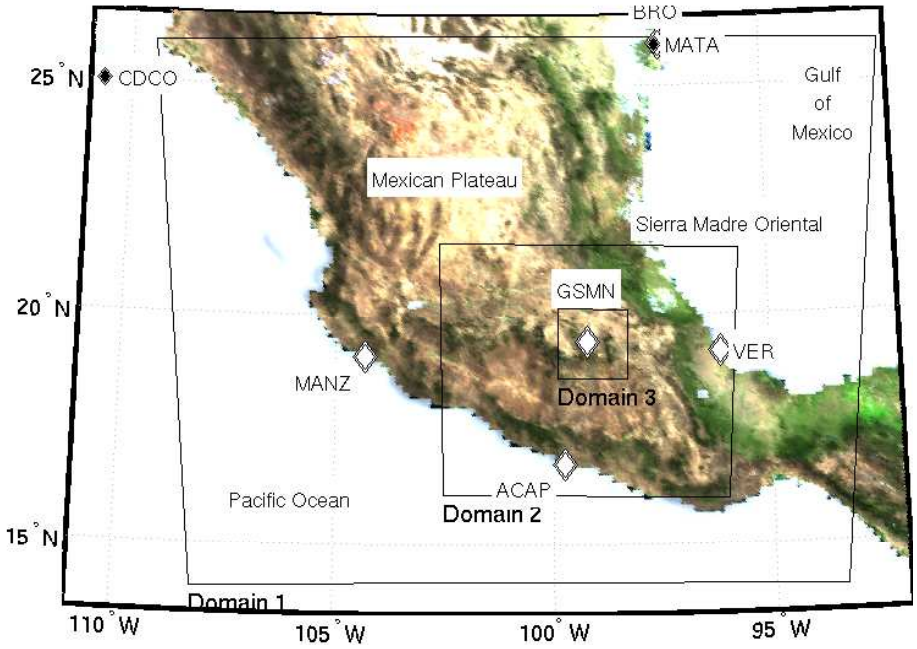

Fig. 1. Map of Mexico showing locations of radiosonde observations: Mexico City (GSMN), Manzanillo (MANZ), Acapulco (ACAP), Veracruz (VER) and Brownsville, Texas (BRO). Also shown are the surface stations Ciudad Constitucion (CDCO) and Matamoros (MATA) and the limits of the 3 MM5 domains.

ACPD

5, 11055–11090, 2005

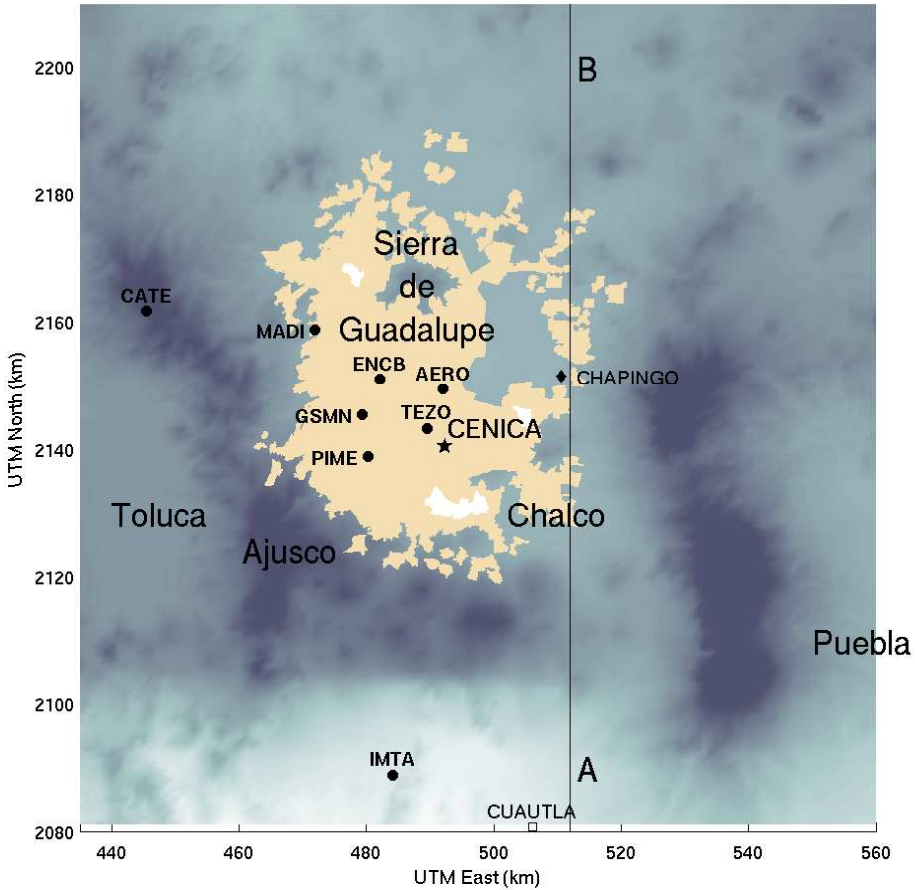

Fig. 2. Map of the Mexico City basin with topography represented by shading and the MCMA (as of 1995) in beige. Campaign supersite was at CENICA. Circles denote SMN stations. Black line A-B is the cross-section used in Fig. 8.

ACPD
5, 11055–11090, 2005

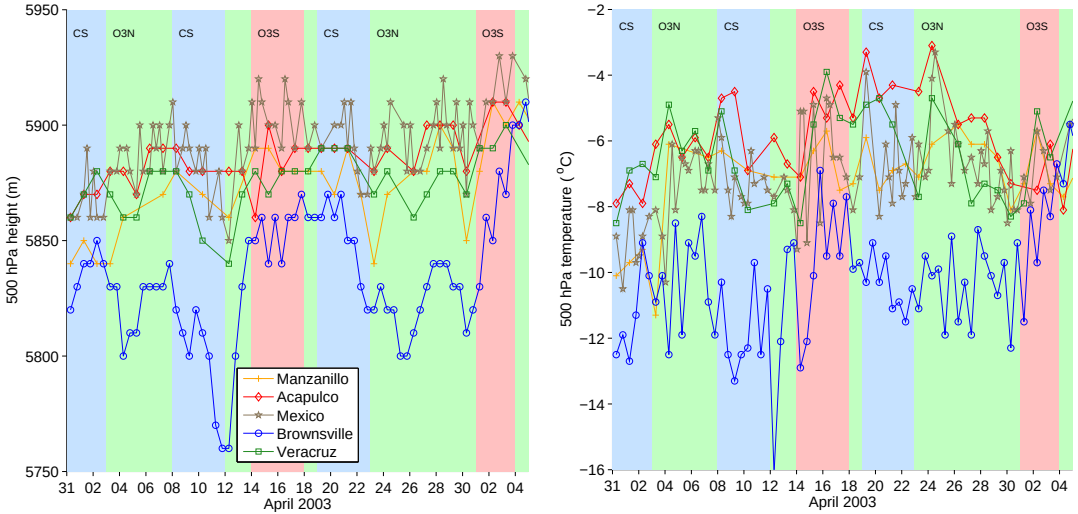

Fig. 3. 500 hPa height and temperature from radiosonde observations during MCMA-2003. Background shading corresponds to episode types: red for O3-South, green for O3-North and blue for Cold Surge.

ACPD
5, 11055–11090, 2005

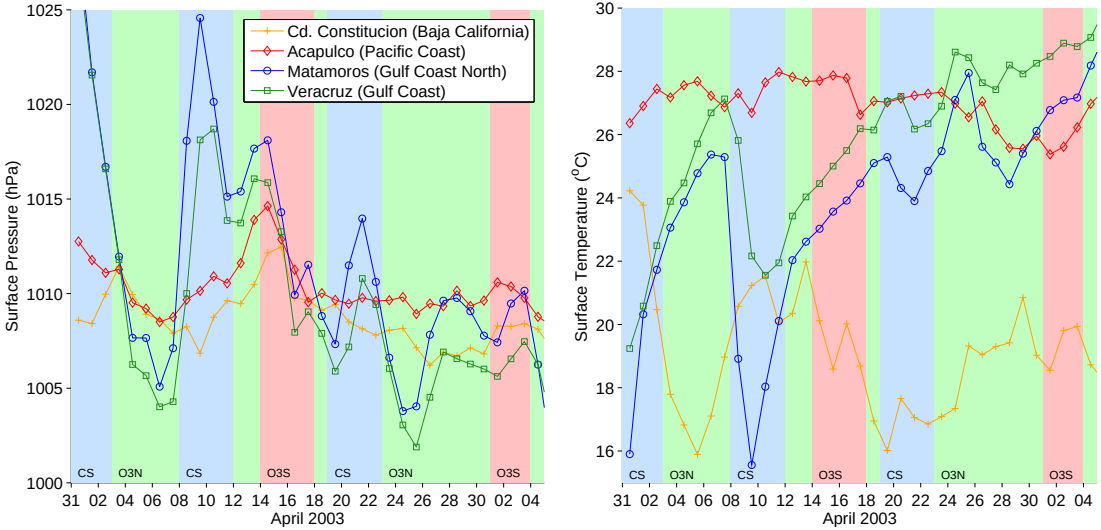

Fig. 4. Daily averaged surface pressure and temperature on the Pacific and Gulf coasts from SMN stations. Shading as for Fig. 3.

ACPD
5, 11055–11090, 2005

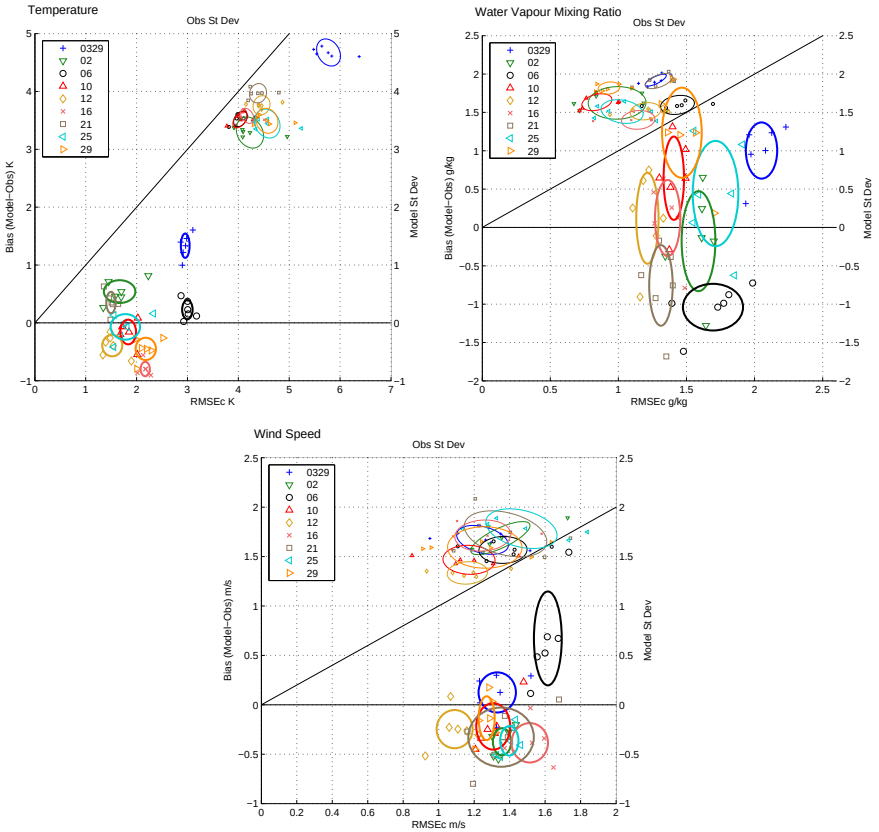

Fig. 5. Statistics diagram for temperature water vapour mixing ratio and wind speed comparing the fine MM5 domain with the 5 SMN surface stations in the basin. Different symbols for each 4 day simulation period labelled by starting day (April except for 0329). Large symbols represent the centred root mean square error (RMSEc) versus the bias. Small symbols represent the standard deviation of the model versus the observations. Ellipses are drawn for each model case centred on the average of all the points and with radii corresponding to the standard deviation.

ACPD
5, 11055–11090, 2005

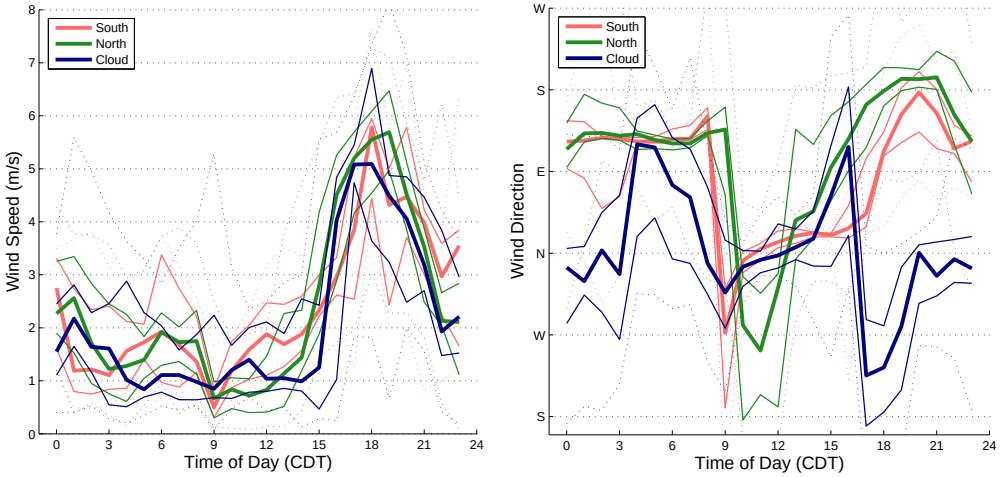

Fig. 6. Simulated diurnal variation of wind speed and direction at CENICA by episode type. Thick line indicates median values, thin lines show the 25 and 75 percentile and dotted lines show minimum and maximum data range.

ACPD
5, 11055–11090, 2005

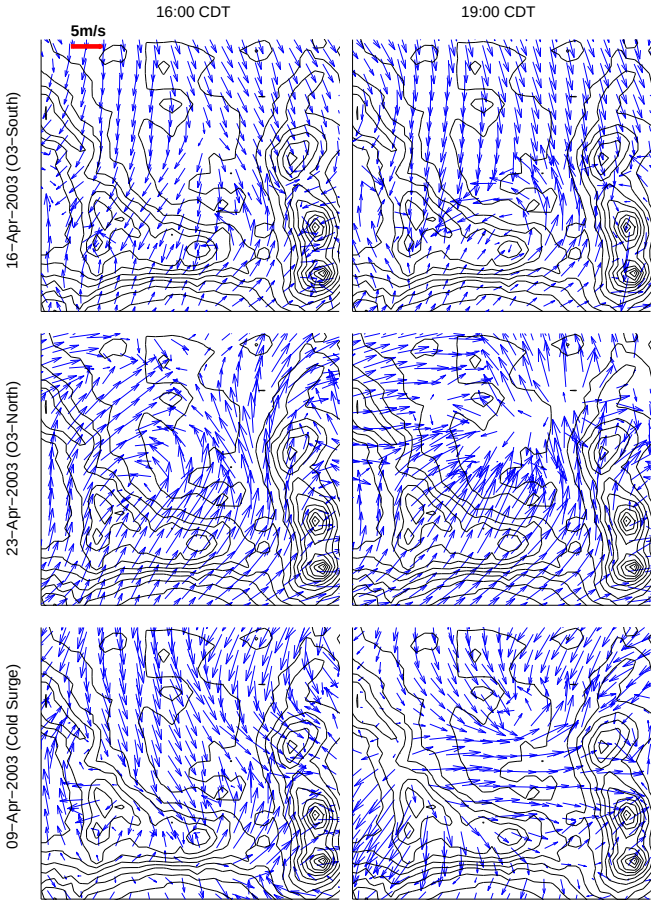

Fig. 7. Horizontal surface (10 m) wind vectors in the Mexico City basin for 16 April (O3-South), 19 April (O3-North) and 9 April (Cold Surge) at 16:00 and 19:00 CDT. Model output with alternate vectors shown only, contour lines of terrain elevation (500 m interval).

ACPD
5, 11055–11090, 2005

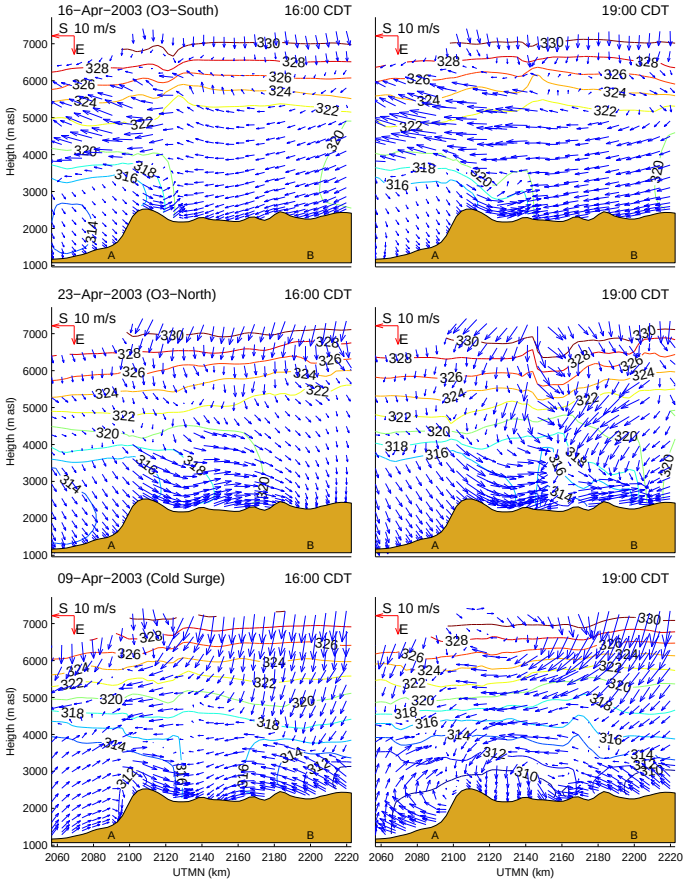

Fig. 8. Vertical cross-section through the Chalco gap and the east side of the basin (line A-B, Fig. 2). Horizontal winds and potential temperature contours (K) depicted for the same times as Fig. 7. Arrows pointing left are westerlies (going East), those pointing down are northerlies (going south, out of the page).

ACPD
5, 11055–11090, 2005

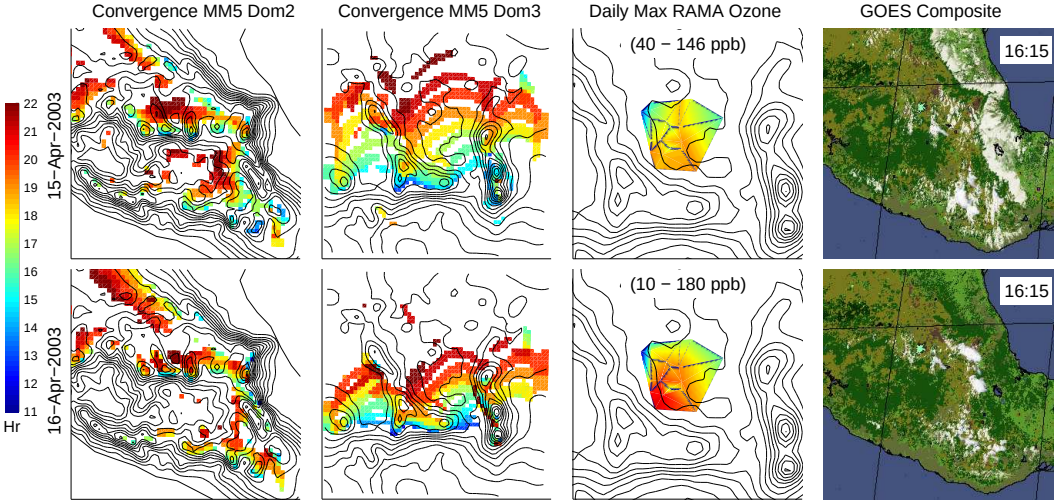

Fig. 9. Convergence lines for O3-South, 15 and 16 April for the medium and fine domain. Each convergence line is coloured by time of day per the colorbar. Surface RAMA ozone concentrations in the basin are shown going from blue to red (highest). GOES cloud imagery for an area similar to the medium domain courtesy of GOES Biomass Burning Monitoring Team, UW-Madison, Cooperative Institute for Meteorological Satellite Studies (CIMSS).

ACPD
5, 11055–11090, 2005

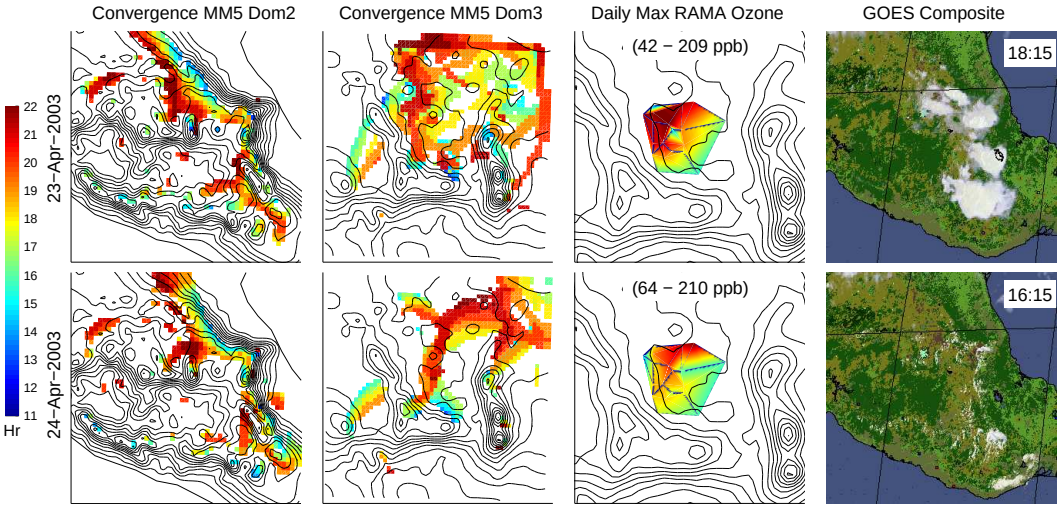

Fig. 10. Convergence lines, ozone and cloud imagery for O3-North, 23 and 24 April, see Fig. 9.

ACPD
5, 11055–11090, 2005

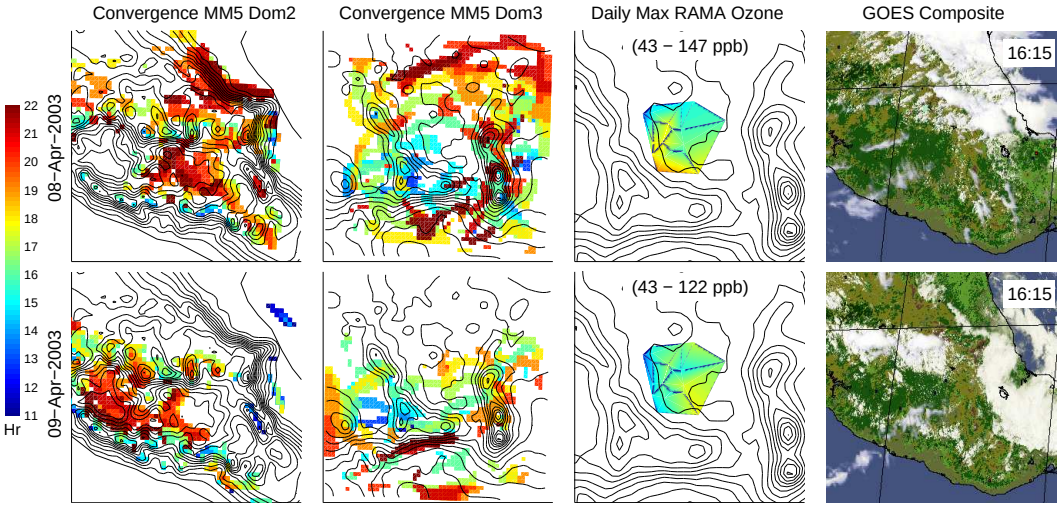

Fig. 11. Convergence lines, ozone and cloud imagery for Cold Surge, 8 and 9 April, see Fig. 9.

ACPD
5, 11055–11090, 2005

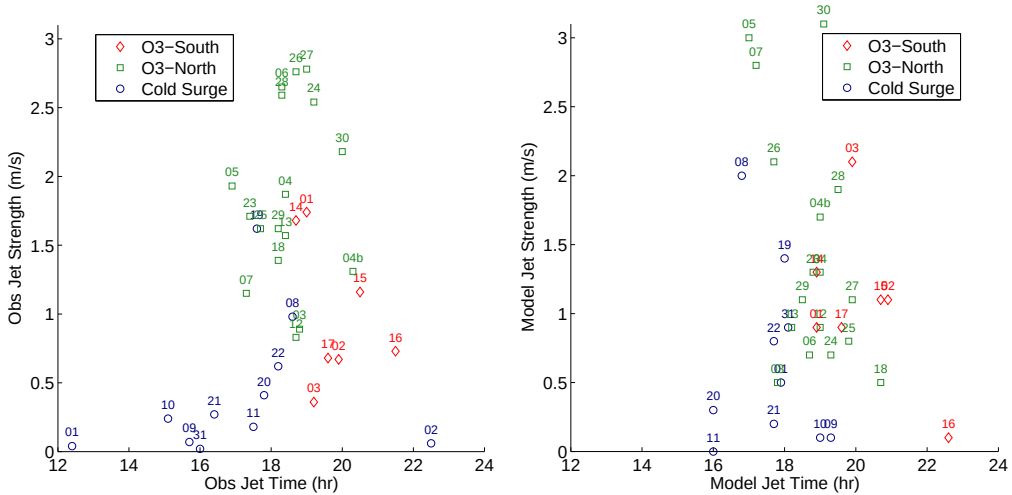

Fig. 12. Jet strength versus jet time for observations and simulations, labelled by day, symbols correspond to episode types (04b is 4 May, others are unambiguously April or May).

ACPD
5, 11055–11090, 2005

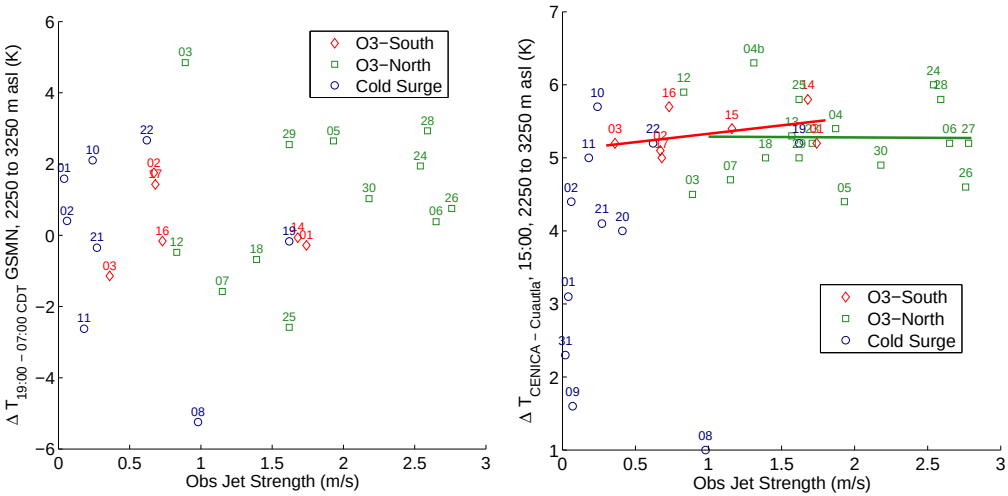

Fig. 13. Temperature differences in the bottom 1000 m versus jet strength. **(a)** Temperature difference at GSMN between 19:00 and 07:00 measured by radiosonde. **(b)** Temperature differences between CENICA and Cuautla, to the south of the gap at 15:00. Lines of best fit from Table 2 shown.

ACPD
5, 11055–11090, 2005

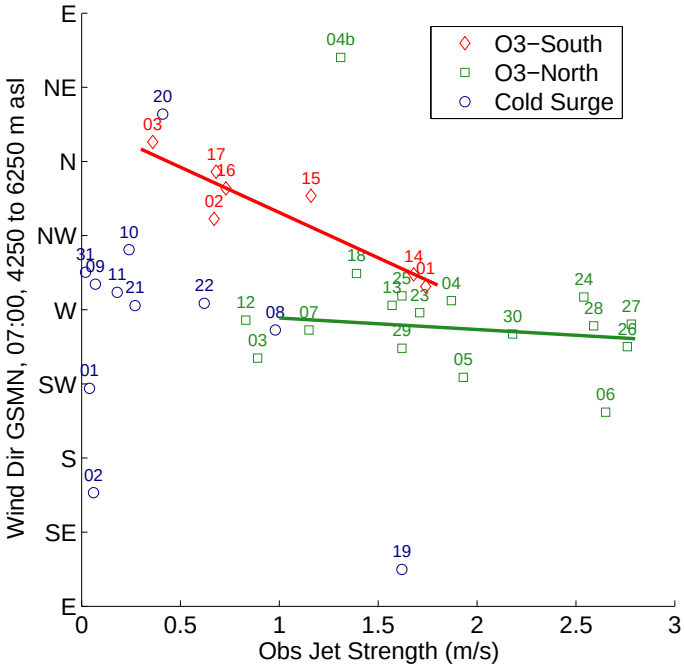

Fig. 14. Wind direction at GSMN at 07:00 averaged between 4250 and 6250 m above sea level versus jet strength. Lines of best fit from Table 2 shown.

ACPD
5, 11055–11090, 2005